

Cavitation instability as a trigger of aneurysm rupture

K. Y. Volokh

Received: 2 November 2014 / Accepted: 22 January 2015 / Published online: 31 January 2015
© Springer-Verlag Berlin Heidelberg 2015

Abstract Aneurysm formation and growth is accompanied by microstructural alterations in the arterial wall. Particularly, the loss of elastin may lead to tissue disintegration and appearance of voids or cavities at the micron scale. Unstable growth and coalescence of voids may be a predecessor and trigger for the onset of macroscopic cracks. In the present work, we analyze the instability of membrane (2D) and bulk (3D) voids under hydrostatic tension by using two experimentally calibrated constitutive models of abdominal aortic aneurysm enhanced with energy limiters. The limiters provide the saturation value for the strain energy, which indicates the maximum energy that can be stored and dissipated by an infinitesimal material volume. We find that the unstable growth of voids can start when the critical stress is considerably less than the aneurysm strength. Moreover, this critical stress may even approach the arterial wall stress in the physiological range. This finding suggests that cavitation instability can be a rational indicator of the aneurysm rupture.

Keywords Aneurysm · Rupture · Instability · Cavitation

1 Introduction

Aneurysms are abnormal dilatations of vessels in the vascular system, and they exist in two major forms such as fusiform and saccular. Fusiform aneurysms are found in the human abdominal aorta. Saccular aneurysms are found in cerebral blood vessels. The Brain Aneurysm Foundation (<http://www.bafound.org/>) reports that two in 100 people in United States have an unruptured brain aneurysm, and the annual

rate of rupture is about 8–10 per 100,000 people. Ruptured brain aneurysms are fatal in about 40 % of cases. Of those who survive, about 66 % suffer some permanent neurological deficit. Similarly, abdominal aortic aneurysm (AAA) is found in ~ 2 % of the elderly population, with $\sim 150,000$ new cases diagnosed each year, and the occurrence is increasing (Bengtsson et al. 1996; Ouriel et al. 1992). In many cases, AAA gradually expands until rupture causing a mortality rate of 90 %. The AAA rupture is considered the 13th most common cause of death in United States (Patel et al. 1995).

Medical doctors consider a surgery option for enlarging AAA, for example, when its maximum diameter reaches 5.5 cm and/or expansion rate is > 1 cm per year. These simplistic geometrical criteria may underestimate the risk of rupture of small aneurysms as well as overestimate the risk of rupture of large aneurysms. Biomechanical approaches to modeling aneurysm evolution are needed and developed, Watton et al. (2004), Baek et al. (2006), Kroon and Holzapfel (2007), Chatziprodromou et al. (2007), Watton et al. (2009), Figueroa et al. (2009), Watton and Hill (2009), Schmid et al. (2010) and Martufi and Gasser (2012) to list a few. Most theories consider the processes of growth and remodeling while the local failure criteria are assumed to be imposed on the results of stress analysis in the spirit of strength-of-materials approach. Alternatively, it is proposed to incorporate a failure description directly in the constitutive equations of both healthy arteries and aneurysms, Volokh (2008a, b, 2010a, 2011a), Volokh and Vorp (2008), Balakhovsky et al. (2014).

Despite the variety of biomechanical models of aneurysm evolution, we still cannot predict rupture. The main reason for that is probably the difficulty in in vivo experimental calibration of theories. This difficulty is obvious and widely appreciated. Less appreciated is the necessity to comprehend possible mechanisms of aneurysm rupture. These mecha-

K. Y. Volokh (✉)
Faculty of Civil and Environmental Engineering,
Technion – I.I.T., Haifa, Israel
e-mail: cvolokh@technion.ac.il

nisms are not evident, and they need to be uncovered. For example, mechanical strength of aneurysms is rather close to the strength of healthy arteries (~ 1.2 MPa) for various arterial locations in human beings and animals (Humphrey 2002; Holzapfel and Ogden 2009; Pierce et al. 2015). The strengths' closeness is truly remarkable because aneurysms undergo significant morphological changes as compared to healthy artery (Vorp 2007; Humphrey and Holzapfel 2012). Intuitively, it is possible to explain the strengths' closeness by the fact that the ultimate stress is controlled by collagen fibers that are present in both aneurysms and healthy arteries. In summary, one cannot claim that the aneurysm rupture is a result of a dramatic decrease in its strength as compared to the healthy arterial wall. In the absence of strength decrease, we should examine failure scenarios related to the presence of small defects.

It is realistic to assume that the healthy arterial wall does not have pronounced defects while the diseased one does. Such defects in the form of voids can appear at the micron scale, for example, when elastin degrades. It is reasonable to assume that the degradation of elastin is accompanied by microstructural rearrangements leaving very small cavities. Such cavities can grow and coalesce in big cavities and, ultimately, in macroscopic cracks. The purpose of the present work was to examine the expansion of small voids in AAA material. Particularly, we analyze the instability of membrane (2D) and bulk (3D) voids under hydrostatic tension by using two experimentally calibrated AAA constitutive models enhanced with energy limiters. The limiters provide the saturation value for the strain energy, which indicates the maximum energy that can be stored and dissipated by an infinitesimal material volume. We find that the unstable growth of voids can start when the critical stress is considerably less than the aneurysm strength. Moreover, this critical stress may even approach the arterial wall stress in the physiological range. This finding suggests that cavitation instability can be a rational indicator of the aneurysm rupture.

2 Hyperelasticity with energy limiters

A variant in the continuum description of bulk failure—*softening hyperelasticity* or *elasticity with energy limiters*—was developed by Volokh (2007, 2010b, 2013, 2014). Softening hyperelasticity is dramatically simpler in formulation than any existing approach for modeling material failure: its basic idea is to introduce an energy limiter in the expression for strain energy. Such limiter enforces saturation—the *failure energy*—in the strain energy function, which indicates the maximum amount of energy that can be stored and dissipated by an infinitesimal material volume during rupture. The limiter induces the strain softening in the constitutive equations *automatically*.

The strain energy function for hyperelastic material with softening can be written in the following general form

$$\psi = \psi^{\text{failure}} - H(\alpha) \psi^{\text{elastic}}(\mathbf{C}), \quad (2.1)$$

$$\psi^{\text{failure}} = \psi^{\text{elastic}}(\mathbf{1}), \quad \text{and} \quad \psi^{\text{elastic}}(\mathbf{C}) \rightarrow 0,$$

$$\text{when } \|\mathbf{C}\| \rightarrow \infty, \quad (2.2)$$

where ψ^{failure} and $\psi^{\text{elastic}}(\mathbf{C})$ designate a constant bulk failure energy and an elastic energy, respectively; $H(z)$ is a unit step function, i.e., $H(z) = 0$ if $z < 0$ and $H(z) = 1$ otherwise; $\mathbf{1}$ is a second-order identity tensor; $\mathbf{C} = \mathbf{F}^T \mathbf{F}$ is the right Cauchy–Green tensor; $\mathbf{F} = \partial \mathbf{y}(\mathbf{x}) / \partial \mathbf{x}$ is the deformation gradient where \mathbf{y} is the current placement of a material point, which occupied position \mathbf{x} in a reference configuration; and $\|\mathbf{C}\| = \text{tr } \mathbf{C}^2$, for example.

The switch parameter $\alpha \in (-\infty, 0]$ is defined by the evolution equation

$$\dot{\alpha} = -H\left(\varepsilon - \psi^{\text{elastic}} / \psi^{\text{failure}}\right), \quad \alpha(t = 0) = 0, \quad (2.3)$$

where $0 < \varepsilon \ll 1$ is a dimensionless tolerance constant.

The physical interpretation of (2.1)–(2.3) is straight: material response is hyperelastic as long as the stored energy is below its limit, ψ^{failure} . When the latter limit is reached, then the stored energy remains constant for the rest of the deformation process, thereby making material healing impossible. Parameter α works as a switch: if $\alpha = 0$, the process is hyperelastic and reversible, and if $\alpha < 0$, the material is irreversibly damaged and the stored energy is dissipated.

Using the dissipation inequality, it is possible to derive constitutive law in the following form (Volokh 2014)

$$\mathbf{P} = -2H(\alpha) \mathbf{F} \frac{\partial \psi^{\text{elastic}}}{\partial \mathbf{C}}, \quad (2.4)$$

where \mathbf{P} is the first Piola–Kirchhoff stress tensor.

The elastic energy can be defined as follows (Volokh 2010b), for example,

$$\psi^{\text{elastic}} = \frac{\Phi}{m} \Gamma\left(\frac{1}{m}, \frac{W^m}{\Phi^m}\right), \quad (2.5)$$

where $\Gamma(s, x) = \int_x^\infty t^{s-1} \exp(-t) dt$ is the upper incomplete gamma function; $W(\mathbf{C})$ is the strain energy of *intact*, i.e., without failure, material and Φ is the energy limiter, which can be calibrated in macroscopic experiments; m is a dimensionless material parameter, which controls sharpness of the transition to material instability on the stress–strain curve. Increasing or decreasing m , it is possible to simulate more or less steep ruptures of the internal bonds accordingly.

Substitution of (2.5) in (2.4) yields

$$\mathbf{P} = 2H(\alpha) \exp\left(-\frac{W^m}{\Phi^m}\right) \mathbf{F} \frac{\partial W}{\partial \mathbf{C}}. \quad (2.6)$$

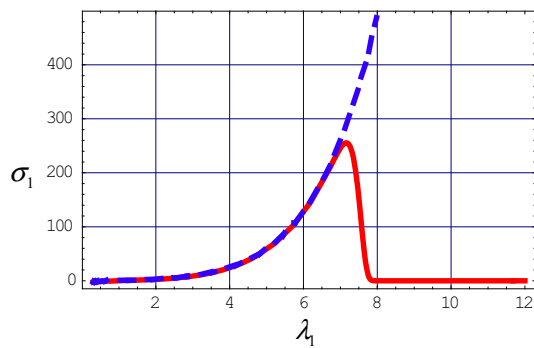


Fig. 1 Cauchy stress (MPa) versus stretch in uniaxial tension of NR: *dashed line* designates the intact model; *solid line* designates the model with energy limiter

Equation (2.5) was specialized for a filled natural rubber (NR) vulcanizate (Volokh 2010b), for example, in the following form

$$\psi^{\text{elastic}} = \frac{\Phi}{10} \Gamma \left(\frac{1}{10}, \frac{W^{10}}{\Phi^{10}} \right), \tag{2.7}$$

$$W = \sum_{k=1}^3 c_k (\text{tr} \mathbf{C} - 3)^k, \quad J = \det \mathbf{F} = 1, \tag{2.8}$$

where $c_1 = 0.298$ MPa, $c_2 = 0.014$ MPa, $c_3 = 0.00016$ MPa, $\Phi = 82.0$ MPa.

The stress–stretch curve for the NR model described by (2.7)–(2.8) is shown in Fig. 1, where also the results are shown for the intact model ($\Phi \rightarrow \infty$). Material failure occurs at the limit point at critical stretch $\lambda_{\text{cr}} = 7.12$ in accordance with the experimental data.

Consequences of the formulation presented by (2.7)–(2.8) are reviewed in Volokh (2013). Here, we only mention two theoretical predictions that can be compared to the experimental data. Figure 2a presents the critical failure stretches in a thin sheet of NR undergoing biaxial tension with different biaxiality ratios. Predictions based on a softening hyperelasticity model are compared to the reported test results. The theoretical model was calibrated in uniaxial tension discussed above, and somewhat lower critical stretches in equal biaxial tension are expected in view of the high imperfection sensitivity of the experiments. Figure 2b presents a cross section of a natural rubber specimen in the “poker-chip” test (Gent and Lindley 1959). The cut was done at the hydrostatic tension of ~ 2.7 MPa. The grown spherical cavities are visible. Softening hyperelasticity model (Volokh 2011b) predicts the onset of instability and growth of the microscopic preexisting cavities at the hydrostatic tension of ~ 2.4 MPa. Both comparisons with the experimental data encourage the use of the methods of energy limiters.

Remark 1 We note that the account of dissipation via step function in (2.1) is necessary when the material unloading

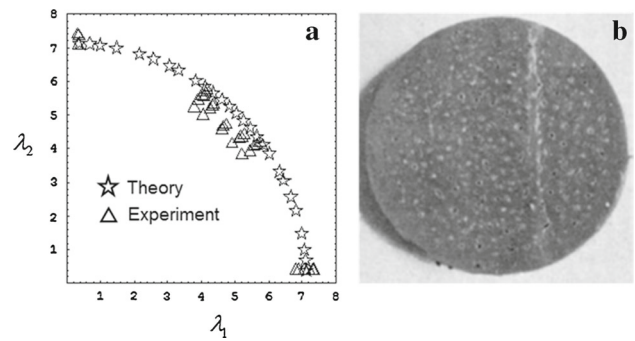


Fig. 2 a Critical failure stretches in biaxial tension for natural rubber; b grown cavities in the poker-chip test

is sound as in the case of crack propagation, for example. Otherwise, the step function can be dropped from equations as in the subsequent analysis of void growth.

3 AAA constitutive models with energy limiters

In this section, we calibrate two constitutive models of AAA incorporating the failure description.

Substitution of (2.5) in (2.1)–(2.2) yields

$$\psi = \frac{\Phi}{m} \Gamma \left(\frac{1}{m}, 0 \right) - H(\alpha) \frac{\Phi}{m} \Gamma \left(\frac{1}{m}, \frac{W^m}{\Phi^m} \right). \tag{3.1}$$

We further assume

$$W = c_1 (\text{tr} \mathbf{C} - 3) + c_2 (\text{tr} \mathbf{C} - 3)^2, \quad \det \mathbf{F} = 1, \tag{3.2}$$

$$m = 1. \tag{3.3}$$

Substituting (3.2)–(3.3) in (3.1) and ignoring unloading (see Remark 1 above), we finally get

$$\psi = \Phi - \Phi \exp \left[- (c_1 (\text{tr} \mathbf{C} - 3) + c_2 (\text{tr} \mathbf{C} - 3)^2) / \Phi \right]. \tag{3.4}$$

This constitutive model has three material constants c_1, c_2, Φ that are fitted to the results of uniaxial tension tests by using a least squares minimization procedure.

The first model—Fig. 3—was calibrated in Volokh and Vorp (2008) as follows:

$$c_1 = 0.103 \text{ MPa}, \quad c_2 = 0.18 \text{ MPa}, \quad \Phi = 0.402 \text{ MPa}. \tag{3.5}$$

The second model based on the Raghavan and Vorp (2000) tests—Fig. 4—is calibrated here as follows:

$$c_1 = 0.52 \text{ MPa}, \quad c_2 = 3.82 \text{ MPa}, \quad \Phi = 0.255 \text{ MPa}. \tag{3.6}$$

We note that the models are different. The first model exhibits softer response with smaller critical stress and greater critical stretch as compared to the second one. We will further use both models to study the void expansion.

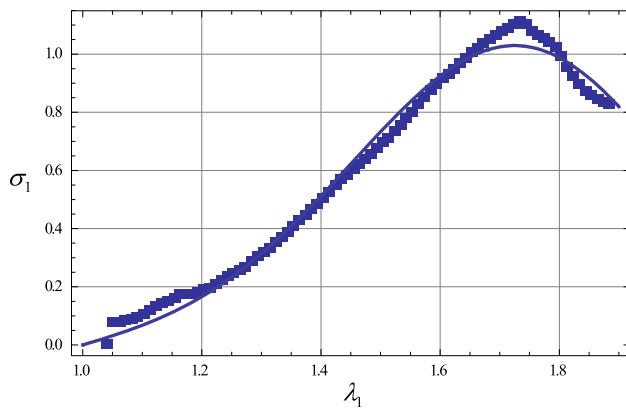


Fig. 3 Cauchy stress (MPa) versus stretch for theory (*solid line*) and experiment (*filled square*) in uniaxial tension for AAA material from Volokh and Vorp (2008)

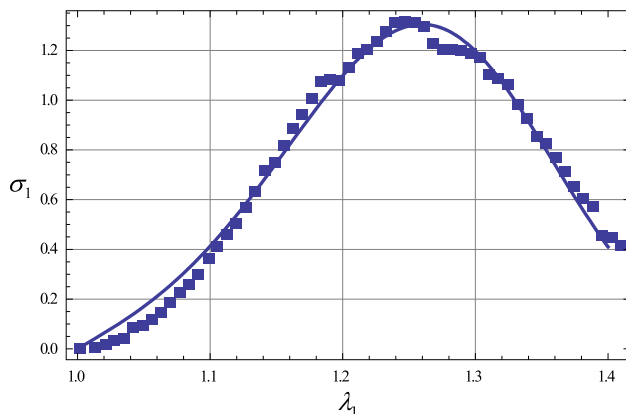


Fig. 4 Cauchy stress (MPa) versus stretch for theory (*solid line*) and experiment (*filled square*) in uniaxial tension for AAA material from Raghavan and Vorp (2000)

It is worth noting also that we use the simplest model (3.2) to intact material behavior in view of the available experimental data. However, the account of the second principal invariant can be relevant for soft materials—see Horgan and Smayda (2012).

Remark 2 Aneurysmal tissues are not ideally isotropic. Perhaps, more developed aneurysms are more isotropic. Recently, Pierce et al. (2015) tested healthy and aneurysmal arterial tissues and calibrated constitutive models in which anisotropy was presented via angle φ that defined directions of two conjugate families of fibers. Testing a number of samples they found the median angles $\varphi_{TAA} = 44.8^\circ$ and $\varphi_{AAA} = 41.9^\circ$ for the thoracic and abdominal aortic aneurysms, respectively. These angles are close to $\varphi = 45^\circ$, which manifests the equivalence of circumferential and longitudinal arterial directions. The latter equivalence is the characteristic of isotropy. It is interesting to note that the corresponding angles for the healthy thoracic and abdominal aorta were not much different: $\varphi_{TA} = 51.0^\circ$ and $\varphi_{AA} = 38.8^\circ$.

4 Expansion of bulk (3D) void

Theoretical considerations of the expansion of bulk voids in various materials have a long history (e.g., Williams and Schapery 1965; Durban and Baruch 1976; Bassani et al. 1980; Ball 1982; Abeyaratne and Horgan 1985; Gent 1990; Huang et al. 1991; Hou and Abeyaratne 1992; Horgan and Polignone 1995; Fond 2001; Lopez-Pamies 2009; Henao 2009; Volokh 2011b). However, nobody (to the best of our knowledge) considered the aneurysmal or arterial tissues. The latter consideration is presented below, and it is based on the approach used in Volokh (2011b).

Assuming that the deformation is centrally symmetric, and the natural base vectors in spherical coordinates coincide with the principal directions of stretches, we can write the deformation law as follows:

$$r = r(R), \quad \vartheta = \Theta, \quad \omega = \Omega, \quad (4.1)$$

where a material particle occupying position (R, Θ, Ω) in the initial configuration is moving to position (r, ϑ, ω) in the current configuration.

Designating the radial direction with index 1 and tangential directions with indices 2 and 3, we can write the principal stretches in the form

$$\lambda_1 = \frac{dr}{dR}, \quad \lambda_2 = \lambda_3 = \frac{r}{R}. \quad (4.2)$$

Since the volume of incompressible material is preserved during deformation, we have

$$b^3 - a^3 = B^3 - A^3, \quad (4.3)$$

where A and a are the internal and B and b are the external radii of the sphere before and after deformation accordingly. We also notice that any sub-sphere with the internal or external radius $r(R)$ should also preserve its volume, and consequently, we get

$$r^3 - a^3 = R^3 - A^3. \quad (4.4)$$

The principal components of the Cauchy stress are in the directions of the natural base vectors

$$\begin{aligned} \sigma_1 = \sigma_{rr} &= -p + \lambda_1 \frac{\partial \psi}{\partial \lambda_1} \\ \sigma_2 = \sigma_{\vartheta\vartheta} &= -p + \lambda_2 \frac{\partial \psi}{\partial \lambda_2} \\ \sigma_3 = \sigma_{\omega\omega} &= -p + \lambda_3 \frac{\partial \psi}{\partial \lambda_3}, \end{aligned} \quad (4.5)$$

where p is indefinite Lagrange multiplier.

The stresses should obey the only equilibrium equation

$$\frac{d\sigma_{rr}}{dr} + 2 \frac{\sigma_{rr} - \sigma_{\vartheta\vartheta}}{r} = 0. \quad (4.6)$$

This equation can be integrated as follows:

$$\sigma_{rr}(b) - \sigma_{rr}(a) = 2 \int_a^b \frac{\sigma_{\vartheta\vartheta} - \sigma_{rr}}{r} dr, \tag{4.7}$$

or

$$g = 2 \int_a^b \left(\lambda_2 \frac{\partial \psi}{\partial \lambda_2} - \lambda_1 \frac{\partial \psi}{\partial \lambda_1} \right) \frac{dr}{r}, \tag{4.8}$$

where boundary conditions have been taken into account

$$\sigma_{rr}(r = a) = 0, \quad \sigma_{rr}(r = b) = g. \tag{4.9}$$

We notice that hydrostatic tension g is a function of the placement of the internal boundary, a , with account of

$$R(r, a) = \sqrt[3]{r^3 - a^3 + A^3}. \tag{4.10}$$

To make the formulation dimensionless with respect to length, we rewrite (4.8) as follows:

$$g = 2 \int_{\bar{a}}^{\bar{b}} \left(\lambda_2 \frac{\partial \psi}{\partial \lambda_2} - \lambda_1 \frac{\partial \psi}{\partial \lambda_1} \right) \frac{d\bar{r}}{\bar{r}}, \tag{4.11}$$

where

$$\lambda_1 = \frac{R^2}{r^2} = \frac{\bar{R}^2}{\bar{r}^2}, \quad \lambda_2 = \lambda_3 = \frac{r}{R} = \frac{\bar{r}}{\bar{R}}, \tag{4.12}$$

$$\bar{r} = \frac{r}{A}, \quad \bar{R} = \frac{R}{A}, \quad \bar{a} = \frac{a}{A}, \quad \bar{b} = \frac{b}{A}, \tag{4.13}$$

$$\bar{R}(\bar{r}, \bar{a}) = \sqrt[3]{\bar{r}^3 - \bar{a}^3 + 1}. \tag{4.14}$$

For $\bar{b} \gg \bar{a}$, we have the problem of the expansion of small void in the infinite medium under the remote hydrostatic tension.¹ The graph defined by (4.11) relates the tension with the void hoop stretch, $\bar{a} = a/A$. The results of the numerical integration of (4.11) are presented in Figs. 5 and 6 for two AAA constitutive models described by equations (3.4), (3.5) and (3.4), (3.6), respectively.

The results show that starting from the hydrostatic tension of 0.38MPa for the first AAA model and 0.81 MPa for the second one, the void expands unstably—it yields. The corresponding critical hoop stretches at the void edge are $a/A = 1.6$ and $a/A = 1.2$. It should not be missed that the unstable yield of the void is a result of the assumption of the centrally symmetric deformation. This assumption is restrictive, of course, and it will be violated for real materials that are not perfect. The latter will trigger the localization of failure in the vicinity of the critical yield point. Nonetheless, the prediction of the critical point of the void instability seems to be reasonable even in the presence of imperfections.

Remark 3 It is worth emphasizing that there is no general agreement on the definition of the cavitation instability, and different authors use different definitions. In the present

¹ In computations, we assumed $\bar{b} = 1,000$.

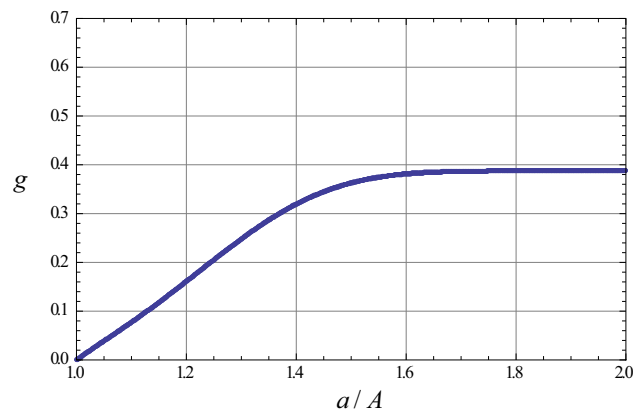


Fig. 5 3D void: hydrostatic tension (MPa) versus hoop stretch for AAA material from Volokh and Vorp (2008)

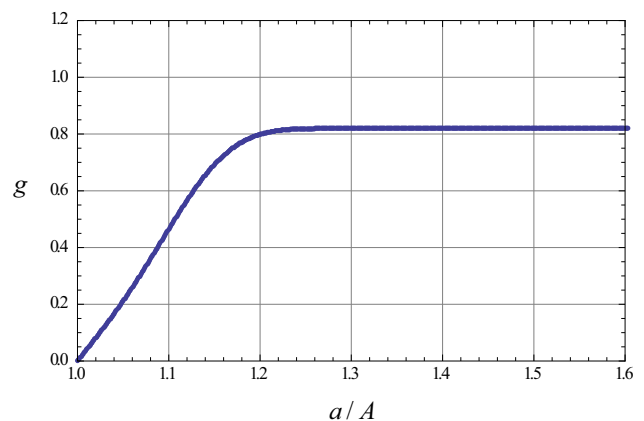


Fig. 6 3D void: hydrostatic tension (MPa) versus hoop stretch for AAA material from Raghavan and Vorp (2000)

work, we define the cavitation instability as an event when the increase in the void size does not require further increase in the load.

5 Expansion of membrane (2D) void

The membrane voids attracted less attention than the bulk ones (e.g., Durban and Birman 1982; Haughton 1986, 1990; Xinchun and Changjun 2002; Cohen and Durban 2010; Volokh 2011b). Again, however, no aneurysmal or arterial tissues were considered. The latter consideration is presented below.

We consider biaxial tension of a membrane disk. By using cylindrical coordinates, we define the referential region occupied by the membrane as follows:

$$A \leq R \leq B, \quad 0 \leq \Theta \leq 2\pi, \quad -H/2 \leq Z \leq H/2. \tag{5.1}$$

The membrane region after the deformation is

$$a \leq r \leq b, \quad 0 \leq \vartheta \leq 2\pi, \quad -h/2 \leq z \leq h/2, \tag{5.2}$$

We assume that the deformation is axisymmetric, and a material particle occupying position (R, Θ, Z) in the reference configuration moves to position (r, ϑ, z) in the current configuration in accordance with the following law

$$r = r(R), \quad \vartheta = \Theta, \quad z = \frac{h(R)}{H} Z. \tag{5.3}$$

Based on (5.3), we calculate the deformation gradient in cylindrical coordinates

$$\mathbf{F} = \frac{dr}{dR} \mathbf{e}_r \otimes \mathbf{E}_R + \frac{r}{R} \mathbf{e}_\vartheta \otimes \mathbf{E}_\Theta + \frac{dh}{dR} \frac{Z}{H} \mathbf{e}_z \otimes \mathbf{E}_R + \frac{h}{H} \mathbf{e}_z \otimes \mathbf{E}_Z, \tag{5.4}$$

where $\{\mathbf{E}_R, \mathbf{E}_\Theta, \mathbf{E}_Z\}$ and $\{\mathbf{e}_r, \mathbf{e}_\vartheta, \mathbf{e}_z\}$ are orthonormal base vectors for reference and current configurations accordingly.

Since the membrane is thin, we use the deformation gradient averaged over thickness

$$\langle \mathbf{F} \rangle = \frac{1}{H} \int_{-H/2}^{H/2} \mathbf{F} dZ = \frac{dr}{dR} \mathbf{e}_r \otimes \mathbf{E}_R + \frac{r}{R} \mathbf{e}_\vartheta \otimes \mathbf{E}_\Theta + \frac{h}{H} \mathbf{e}_z \otimes \mathbf{E}_Z. \tag{5.5}$$

We notice that the transition from (5.3) to (5.4) brings a great simplification since the directions of the base vectors in cylindrical coordinates coincide with the average principal stretches. Based on (5.5) and designating the radial, tangential, and lateral directions with indices 1, 2, and 3, respectively, we can write the average principal stretches in the form

$$\lambda_1 = \frac{dr}{dR}, \quad \lambda_2 = \frac{r}{R}, \quad \lambda_3 = \frac{h}{H}. \tag{5.6}$$

The constitutive equations relate the average stretches to the components of the 1st Piola–Kirchhoff stress tensor \mathbf{P} , as follows:

$$\begin{aligned} P_1 &= P_{rR} = \frac{\partial \psi}{\partial \lambda_1} - p \lambda_1^{-1} \\ P_2 &= P_{\vartheta\Theta} = \frac{\partial \psi}{\partial \lambda_2} - p \lambda_2^{-1} \\ P_3 &= P_{zZ} = \frac{\partial \psi}{\partial \lambda_3} - p \lambda_3^{-1}, \end{aligned} \tag{5.7}$$

where p is the indefinite Lagrange multiplier enforcing the incompressibility condition

$$\lambda_1 \lambda_2 \lambda_3 = 1. \tag{5.8}$$

Since the membrane faces are stress-free, $P_{zZ} = 0$, we can exclude the Lagrange multiplier from (5.7)

$$\begin{aligned} P_1 &= P_{rR} = \frac{\partial \psi}{\partial \lambda_1} - \frac{\lambda_3}{\lambda_1} \frac{\partial \psi}{\partial \lambda_3} \\ P_2 &= P_{\vartheta\Theta} = \frac{\partial \psi}{\partial \lambda_2} - \frac{\lambda_3}{\lambda_2} \frac{\partial \psi}{\partial \lambda_3} \end{aligned} \tag{5.9}$$

It is worth reminding again that the principal values of the first Piola–Kirchhoff stress tensor correspond to the thickness average stretches.

Now, the equilibrium equations with respect to referential coordinates (Volokh 2006) reduce to

$$\frac{dP_1}{dR} + \frac{P_1 - P_2}{R} = 0. \tag{5.10}$$

This equation is completed by the conditions at the membrane edges

$$P_1(A) = 0, \quad P_1(B) \lambda_1(B) = g, \tag{5.11}$$

where g is the value of the hydrostatic tension.

Normalizing the length scale by the radius of the initial cavity, we introduce

$$\begin{aligned} \lambda_1 &= \frac{d\bar{r}}{d\bar{R}} = \frac{dr}{dR}, \quad \lambda_2 = \frac{\bar{r}}{\bar{R}} = \frac{r}{R}, \\ \lambda_3 &= \frac{\bar{h}}{\bar{H}} = \frac{h}{H}, \end{aligned} \tag{5.12}$$

$$\begin{aligned} \bar{r} &= \frac{r}{A}, \quad \bar{R} = \frac{R}{A}, \quad \bar{h} = \frac{h}{A}, \quad \bar{H} = \frac{H}{A}, \quad \bar{A} = 1, \\ \bar{B} &= \frac{B}{A}. \end{aligned} \tag{5.13}$$

Substituting (5.12)–(5.13) in (5.10)–(5.11), we obtain the two-point boundary value problem

$$\frac{dP_1}{d\bar{R}} + \frac{P_1 - P_2}{\bar{R}} = 0, \tag{5.14}$$

$$P_1(1) = 0, \quad P_1(\bar{B}) \lambda_1(\bar{B}) = g, \tag{5.15}$$

where the principal stresses are defined in (5.9) and principal stretches are defined in (5.12) with account of the incompressibility condition (5.8).

Equation (5.14) and boundary conditions (5.15) can be solved numerically for $\bar{r}(\bar{R})$ with account of (5.8), (5.9), and (5.12). In the case of $\bar{B} \gg 1$, we have the problem of the expansion of small void in the infinite membrane under the biaxial tension.²

Since our purpose was to track the stress–stretch curve, there is no need to solve the two-point boundary value problem for the given hydrostatic tension, g . Instead, it is reasonable to solve a simpler initial value problem defined by the following conditions at point $\bar{A} = 1$:

$$\bar{r}(1) = \frac{a}{A}, \quad \frac{d\bar{r}}{d\bar{R}}(1) = \beta. \tag{5.16}$$

Here, β is defined from (5.15)₁ by solving the algebraic equation

$$\frac{\partial \psi}{\partial \lambda_1} - \frac{\lambda_3}{\lambda_1} \frac{\partial \psi}{\partial \lambda_3} = 0, \tag{5.17}$$

² In computations, we assumed $\bar{B} = 1,000$.

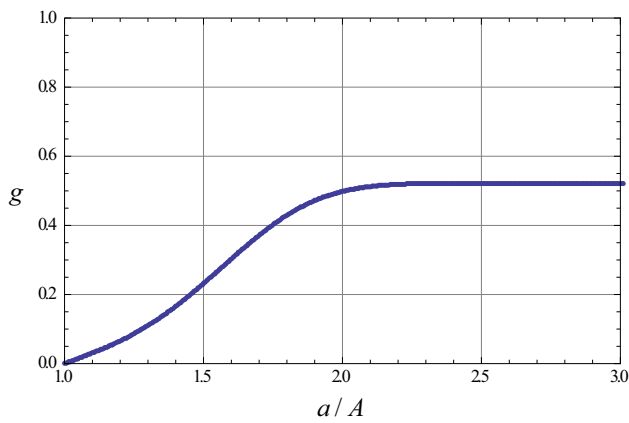


Fig. 7 2D void: hydrostatic tension (MPa) versus hoop stretch for AAA material from Volokh and Vorp (2008)

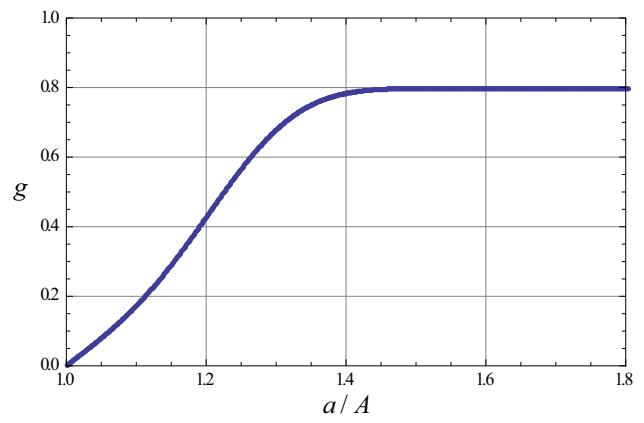


Fig. 8 2D void: hydrostatic tension (MPa) versus hoop stretch for AAA material from Raghavan and Vorp (2000)

where

$$\lambda_1 = \beta, \quad \lambda_2 = \frac{a}{A}, \quad \lambda_3 = \frac{1}{\lambda_1 \lambda_2}. \tag{5.18}$$

By the direct calculation, we obtain

$$\frac{\partial \psi}{\partial \lambda_1} = \frac{\partial \psi}{\partial W} \frac{\partial W}{\partial \lambda_1} = \frac{\partial \psi}{\partial W} 2\lambda_1 \sum_{k=1}^2 k c_k (\lambda_1^2 + \lambda_2^2 + \lambda_3^2 - 3)^{k-1}, \tag{5.19}$$

$$\frac{\partial \psi}{\partial \lambda_3} = \frac{\partial \psi}{\partial W} \frac{\partial W}{\partial \lambda_3} = \frac{\partial \psi}{\partial W} 2\lambda_3 \sum_{k=1}^2 k c_k (\lambda_1^2 + \lambda_2^2 + \lambda_3^2 - 3)^{k-1}. \tag{5.20}$$

Substituting (5.19)–(5.20) in (5.17), we get

$$\lambda_1^2 = \lambda_3^2, \tag{5.21}$$

Finally, substituting (5.18) in (5.21), we have

$$\beta = \sqrt{\frac{A}{a}}. \tag{5.22}$$

Now, the solution of (5.14) and (5.16) can be generated numerically for varying a , and g is the outcome of the calculation—Figs. 7 and 8.

The results show that starting from tension of 0.46 MPa for the first AAA model and 0.8 MPa for the second one, the void expands in the unstable mode.

6 Discussion

This study is a step toward clarification of a possible mechanism of aneurysm rupture. Classical approaches for modeling aneurysm are based on the stress analysis of evolving tissue. In the ideal case of larger aneurysm diameter and smaller thickness, as compared to the healthy artery, the wall stress

should significantly increase. However, the real wall evolution is accompanied by the formation of thrombus and other morphological changes that lead to wall thickening and stress reduction (e.g., Vorp 2007). Thus, generally the existing models might fail to reveal the process of mechanical rupture. It is remarkable that experiments with aneurysmal tissue show strength similar to healthy arteries (~1.2 MPa). Therefore, it is hardly possible to directly connect the aneurysm failure to the tissue degradation. Indeed, collagen fibers—the main load-bearing part of the arterial wall—are present in both healthy and diseased tissue. This situation requires account of microscopic defects in order to understand the mechanics of aneurysm failure.

In the present work, we assumed that degradation of elastin was accompanied by microstructural rearrangements leaving very small cavities in aneurysmal tissue. Such cavities can grow and coalesce in big cavities and, ultimately, in macroscopic cracks. We analyzed the instability of membrane (2D) and bulk (3D) cavities under hydrostatic tension by using two experimentally calibrated AAA constitutive models enhanced with energy limiters. The limiters provided the saturation value for the strain energy, which indicated the maximum energy that could be stored and dissipated by an infinitesimal material volume.

We found that the unstable growth of cavities could start when the critical stress was considerably less than the aneurysm strength. For example, the critical stress for the 3D cavity of the first AAA model (~0.4 MPa) approaches the arterial wall stress in the physiological range (~0.2 MPa) (Humphrey et al. 2014). Of course, this result is very material-specific: some cavities might be prone to unstable expansion at stresses close to the physiological range while others not.

We should finally note that the proposed failure mechanism is not necessarily unique, and other factors can be important. For example, microcalcification can be important because it creates stiff particles inside soft tissue. Such parti-

cles can lead to the overall tissue stiffening while locally they can produce high stress/strain concentration. Actually, three-dimensional hydrostatic tension triggering void growth can occur in the vicinity of rigid inclusions. In the presence of rigid particles, the particle–tissue deboning mechanism can also become sound. All mentioned mechanisms, as well as fatigue, take place in materials varying from ductile metals to soft rubbers, and they also should be examined with regard to soft biological tissues including aneurysms.

Acknowledgments Kind assistance of Dr. Shmuel Pinkert with handling graphical data is gratefully appreciated.

References

- Abeyaratne R, Horgan CO (1985) Initiation of localized plane deformations at a circular cavity in an infinite compressible nonlinearly elastic medium. *J Elast* 15:243–256
- Baek S, Rajagopal KR, Humphrey JD (2006) A theoretical model of enlarging intracranial fusiform aneurysms. *J Biomech Eng* 128:142–149
- Balakhovskiy K, Jabareen M, Volokh KY (2014) Modeling rupture of growing aneurysms. *J Biomech* 43:653–658
- Ball JM (1982) Discontinuous equilibrium solutions and cavitation in nonlinear elasticity. *Philos Trans R Soc Lond Ser A Math Phys Eng Sci* 306:557–611
- Bassani JL, Durban D, Hutchinson JW (1980) Bifurcation of a spherical hole in an infinite elastoplastic medium. *Math Proc Camb Philos Soc* 87:339–356
- Bengtsson H, Sonesson B, Bergqvist D (1996) Incidence and prevalence of abdominal aortic aneurysms, estimated by necropsy studies and population screening by ultrasound. *Ann NY Acad Sci* 800:1–24
- Chatziprodromou I, Tricoli A, Poulikakos D, Ventikos Y (2007) Hemodynamic and wall remodeling of a growing cerebral aneurysm: a computational model. *J Biomech* 40:412–426
- Cohen T, Durban D (2010) Cavitation in elastic and hyperelastic sheets. *Int J Eng Sci* 48:52–66
- Durban D, Baruch M (1976) On the problem of a spherical cavity in an infinite elasto-plastic medium. *J Appl Mech* 43:633–638
- Durban D, Birman V (1982) On the elasto-plastic stress concentration at a circular hole in an anisotropic sheet. *Acta Mech* 43:73–84
- Figueroa CA, Baek S, Taylor CA, Humphrey JD (2009) A computational framework for fluid–solid-growth modeling in cardiovascular simulations. *Comput Methods Appl Mech Eng* 198:3583–3602
- Fond C (2001) Cavitation criterion for rubber materials: a review of void-growth models. *J Polym Sci Part B Polym Phys* 39:2081–2096
- Gent AN (1990) Cavitation in rubber: a cautionary tale. *Rubber Chem Technol* 63:G49–G53
- Gent AN, Lindley PB (1959) Internal rupture of bonded rubber cylinders in tension. *Proc R Soc A* 2:195–205
- Haughton DM (1986) On non-existence of cavitation in incompressible elastic membranes. *Q J Mech Appl Math* 39:289–296
- Haughton DM (1990) Cavitation in compressible elastic membranes. *Int J Eng Sci* 28:163–168
- Henao D (2009) Cavitation, invertibility, and convergence of regularized minimizers in nonlinear elasticity. *J Elast* 94:55–68
- Holzappel GA, Ogden RW (eds) (2009) *Biomechanical modelling at the molecular, cellular and tissue levels*. Springer, New York
- Hou H-S, Abeyaratne R (1992) Cavitation in elastic and elastic–plastic solids. *J Mech Phys Solids* 40:571–592
- Horgan CO, Polignone DA (1995) Cavitation in nonlinearly elastic solids: a review. *Appl Mech Rev* 48:471–485
- Horgan CO, Smayda MG (2012) The importance of the second strain invariant in the constitutive modeling of elastomers and soft biomaterials. *Mech Mater* 51:43–52
- Huang Y, Hutchinson JW, Tvergaard V (1991) Cavitation instabilities in elastic–plastic solids. *J Mech Phys Solids* 39:223–241
- Humphrey JD (2002) *Cardiovascular solid mechanics: cells, tissues, and organs*. Springer, New York
- Humphrey JD, Milewicz DM, Tellides G, Schwartz MA (2014) Disfunctional mechanosensing in aneurysms. *Science* 344:477–479
- Humphrey JD, Holzappel GA (2012) Mechanics, mechanobiology, and modeling of human abdominal aorta and aneurysms. *J Biomech* 45:805–814
- Kroon M, Holzappel GA (2007) A model of saccular cerebral aneurysm growth by collagen fiber remodeling. *J Theor Biol* 247:775–787
- Lopez-Pamies O (2009) Onset of cavitation in compressible, isotropic, hyperelastic solids. *J Elast* 94:115–145
- Martufi G, Gasser TC (2012) Turnover of fibrillar collagen in soft biological tissue with application to the expansion of abdominal aortic aneurysms. *J R Soc Interface* 9:3366–3377
- Ouriel K, Green RM, Donayre C, Shortell CK, Elliott J, DeWeese JA (1992) An evaluation of new methods of expressing aortic aneurysm size: relationship to rupture. *J Vasc Surg* 15:12–20
- Patel MI, Hardman DT, Fisher CM, Appleberg M (1995) Current views on the pathogenesis of abdominal aortic aneurysms. *J Am Coll Surg* 181:371–382
- Pierce DM, Maier F, Weisbecker H, Viertler C, Verbrugge P, Famaey N, Fourneau I, Herijgers P, Holzappel GA (2015) Human thoracic and abdominal aortic aneurysmal tissue: damage experiments, statistical analysis and constitutive equations. *J Mech Behav Biomed Mater* 41:92–107
- Raghavan ML, Vorp DA (2000) Toward a biomechanical tool to evaluate rupture potential of abdominal aortic aneurysm: identification of a finite strain constitutive model and evaluation of its applicability. *J Biomech* 33:475–482
- Schmid H, Watton PN, Maurer MM, Wimmer J, Winkler P, Wang YK, Rohrlé O, Itskov M (2010) Impact of transmural heterogeneities on arterial adaptation: application to aneurysm formation. *Biomech Model Mechanobiol* 9:295–315
- Volokh KY (2006) Lagrangian equilibrium equations in cylindrical and spherical coordinates. *Comput Mater Continua* 3:37–42
- Volokh KY (2007) Hyperelasticity with softening for modeling materials failure. *J Mech Phys Solids* 55:2237–2264
- Volokh KY (2008a) Prediction of arterial failure based on a microstructural bi-layer fiber-matrix model with softening. *J Biomech* 41:447–453
- Volokh KY (2008b) Fung’s arterial model enhanced with a failure description. *Mol Cell Biomech* 5:207–216
- Volokh KY (2010a) Comparison of biomechanical failure criteria for abdominal aortic aneurysm. *J Biomech* 43:2032–2034
- Volokh KY (2010b) On modeling failure of rubberlike materials. *Mech Res Commun* 37:684–689
- Volokh KY (2011a) Modeling failure of soft anisotropic materials with application to arteries. *J Mech Behav Biomed Mater* 4:1582–1594
- Volokh KY (2011b) Cavitation instability in rubber. *Int J Appl Mech* 3:299–311
- Volokh KY (2013) Review of the energy limiters approach to modeling failure of rubber. *Rubber Chem Technol* 86:470–487
- Volokh KY (2014) On irreversibility and dissipation in hyperelasticity with softening. *J Appl Mech* 86:470–487
- Volokh KY, Vorp DA (2008) A model of growth and rupture of abdominal aortic aneurysm. *J Biomech* 41:1015–1021
- Vorp DA (2007) Biomechanics of abdominal aortic aneurysm. *J Biomech* 40:1887–1902

- Watton PN, Hill NA (2009) Evolving mechanical properties of a model of abdominal aortic aneurysm. *Biomech Model Mechanobiol* 8:25–42
- Watton PN, Hill NA, Heil M (2004) A mathematical model for the growth of the abdominal aortic aneurysm. *Biomech Model Mechanobiol* 3:98–113
- Watton PN, Ventikos Y, Holzapfel GA (2009) Modeling the growth and stabilization of cerebral aneurysm. *Math Med Biol* 26:133–164
- Williams ML, Schapery RA (1965) Spherical flaw instability in hydrostatic tension. *Int J Fract* 1:64–72
- Xinchun S, Changjun C (2002) Cavitation in Hookean elastic membranes. *Acta Mech Solid Sin* 15:89–94